Inorganic Chemistry

including bioinorganic chemistry

December 2, 2013
Volume 52, Number 23
pubs.acs.org/IC

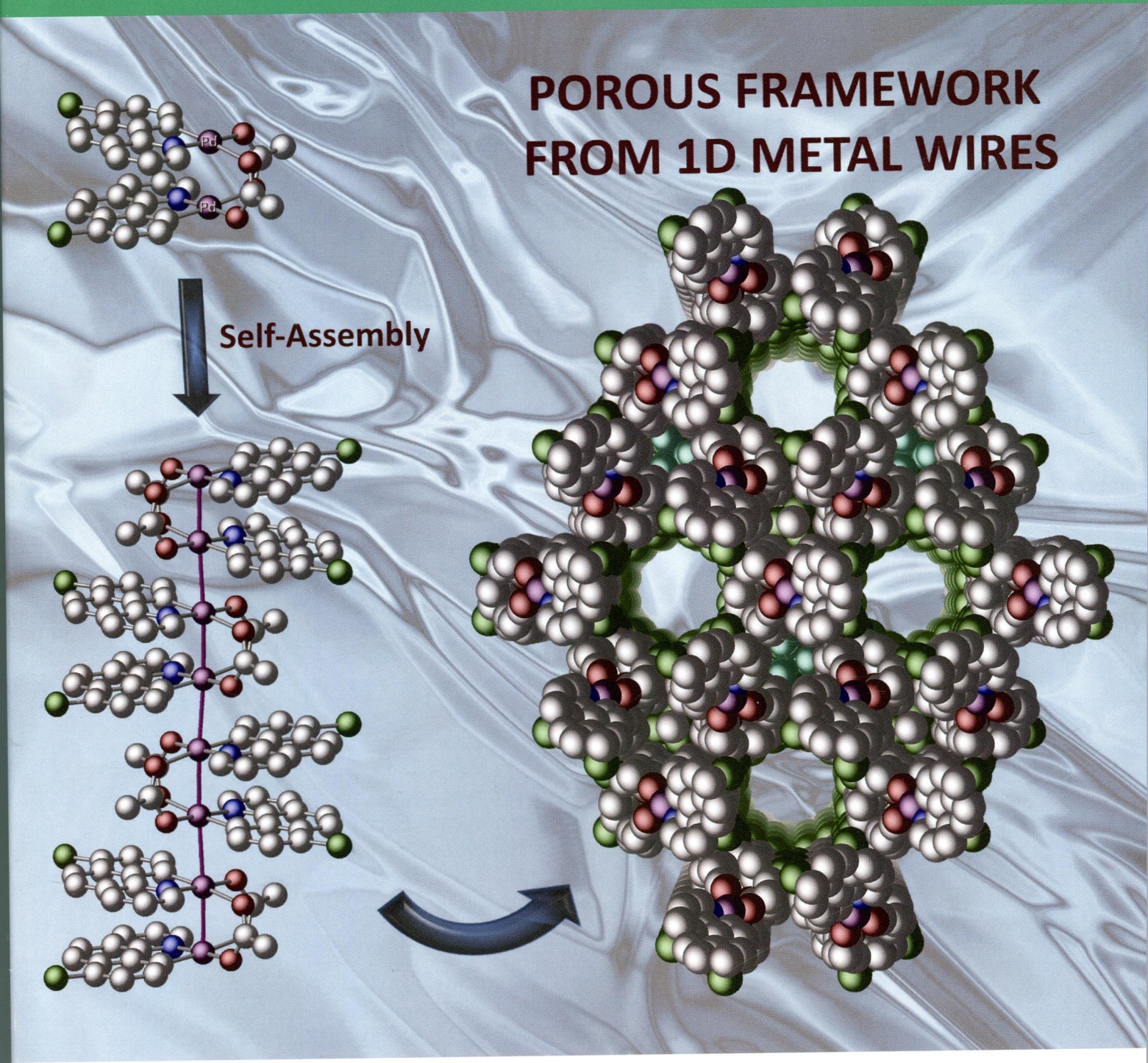

ACS Publications
MOST TRUSTED. MOST CITED. MOST READ.

www.acs.org

Inorganic Chemistry

DECEMBER 2, 2013
VOLUME 52 ISSUE 23

INOCAJ 52(23) 13289−13802 (2013)
ISSN 0020-1669
Registered in the U.S. Patent and Trademark Office

ON THE COVER: Controlled molecular changes are used to influence the supramolecular structures of self-assembled 1D palladium wires, resulting in a porous framework with 1D channels parallel to the palladium chains. See M. G. Campbell, S.-L. Zheng, and T. Ritter, p 13295.

Communications

13289 S dx.doi.org/10.1021/ic401911g

$NdNiMg_5$, a New Magnesium-Rich Phase with an Unusual Structural Type
Bassem Ourane, Etienne Gaudin,* Ridha Zouari, Samuel Couillaud, and Jean-Louis Bobet

The structure of the new Mg-rich phase $NdNiMg_5$ is made of Mg blocks, with a close-packed array of Mg atoms, stacked along the *c* axis. These blocks are separated by NiNd layers and connected through short Mg−Mg bonds. In the NiNd layer, the Ni and Nd atoms form an ordered graphite-type network. Antiferromagnetic ordering is observed with T_N = 12 K.

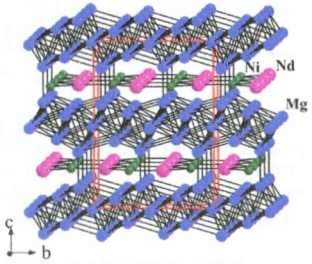

13292 S dx.doi.org/10.1021/ic4019508

Non-Heme Mononitrosyldiiron Complexes: Importance of Iron Oxidation State in Controlling the Nature of the Nitrosylated Products
Amit Majumdar and Stephen J. Lippard*

Iron-oxidation-state-controlled synthesis, characterization, and reactivity of mononitrosyldiiron complexes having $[Fe^{III}\cdot\{FeNO\}^7]$ and $[Fe^{II}\cdot\{FeNO\}^7]$ core formulations in a dinucleating multidentate ligand platform are shown.

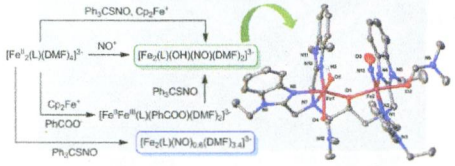

13295 S dx.doi.org/10.1021/ic4019635

One-Dimensional Palladium Wires: Influence of Molecular Changes on Supramolecular Structure

Michael G. Campbell, Shao-Liang Zheng, and Tobias Ritter*

One-dimensional (1D) metal wires featuring metal–metal bonds have been studied for over a century; however, there is a lack of synthetic methods that allow for variation of structure and therefore properties. Here we report the use of molecular control elements to alter the sold-state structures of 1D palladium wires, including Pd–Pd bond distances and the porosity of the supramolecular framework.

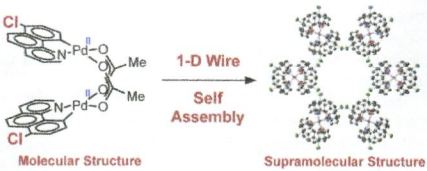

13298 S dx.doi.org/10.1021/ic402391f

"Criss-Crossed" Dinucleating Behavior of an N4 Schiff Base Ligand: Formation of a μ-OH,μ-O_2 Dicobalt(III) Core via O_2 Activation

Yae In Cho, David M. Joseph, and Michael J. Rose*

A "cat's cradle" type of dicobalt(III) complex has been isolated: a μ-hydroxo,μ-peroxo motif is supported by two enN4 (Schiff base) ligands that span both cobalt ions in criss-crossed fashion. The unique cochelated nature of the complex stabilizes reversible Co^{III}–Co^{III}↔Co^{III}–Co^{IV} processes (electrochemically) and enables EPR detection of a formally Co^{III}–Co^{IV} species. DFT calculations support the assignment as either a mixed valence Co^{III}–Co^{IV} configuration or a Co^{III}–Co^{III} species with a bridging superoxo ($O_2^{\bullet-}$) ligand.

13301 S dx.doi.org/10.1021/ic402652t

Perdeuterated 2,2′-Bipyridine-6,6′-dicarboxylate: An Extremely Efficient Sensitizer for Thulium Luminescence in Solution

Jessica Wahsner and Michael Seitz*

A very efficient chelator motif for the sensitization of thulium luminescence in solution has been identified. Straightforward perdeuteration of the ligand scaffold allows the realization of quantum yields greater than $\Phi = 0.12\%$ and luminescence lifetimes of up to $\tau = 4.6$ μs in deuterated solvents.

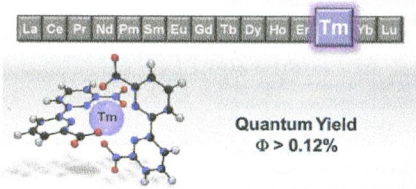

Articles

13304 (S) dx.doi.org/10.1021/ic401802s

Influence of Cation Substitution and Activator Site Exchange on the Photoluminescence Properties of Eu^{3+}-Doped Quaternary Pyrochlore Oxides

S. K. Mahesh, P. Prabhakar Rao,* Mariyam Thomas, T. Linda Francis, and Peter Koshy

Stannate-based pyrochlore-type red phosphors $CaGd_{1-x}SnNbO_7{:}xEu^{3+}$, $Ca_{1-y}Sr_yGd_{1-x}$ $SnNbO_7{:}xEu^{3+}$, and $Ca_{0.8-x}Sr_{0.2}GdSnNbO_{7+\delta}$: xEu^{3+} were prepared via conventional solid-state method. Our results suggest that the photoluminescence properties can be enhanced by simple compositional adjustments in the quaternary pyrochlore-type red phosphors.

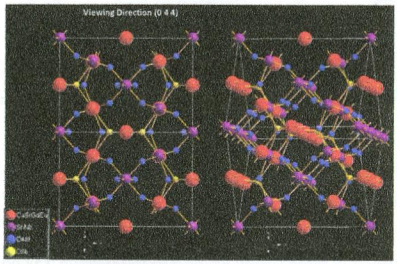

13314 (S) dx.doi.org/10.1021/ic4006828

New Supramolecular Structural Motif Coupling a Ruthenium(II) Polyazine Light Absorber to a Rhodium(I) Center

Rongwei Zhou, Baburam Sedai, Gerald F. Manbeck, and Karen J. Brewer*

A detailed analysis of the redox, spectroscopic, emission, reactivity, and photochemical properties of the new Ru(II),Rh(I) motif via the preparation of new complexes $[(bpy)_2Ru(dpp)Rh^I(COD)]^{3+}$ and $[(Me_2bpy)_2Ru(dpp)Rh^I(COD)]^{3+}$ is reported. The complex has steric repulsion between the alkene COD protons and the pyrazine dpp protons, leading to equilibrium mixtures of Ru(II),Rh(I) with Ru(II) and Rh(I) monometallics in coordinating solvents. The Ru(II),Rh(I) motif is stabilized in noncoordinating solvents, allowing detailed studies of the properties of this motif.

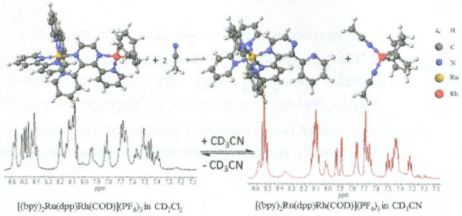

13325 S dx.doi.org/10.1021/ic4010906

Isolation and Characterization of a Dihydroxo-Bridged Iron(III,III)(μ-OH)$_2$ Diamond Core Derived from Dioxygen

Michael K. Coggins, Santiago Toledo, and Julie A. Kovacs*

An Fe(II) complex **1** is reported that reacts with $^{18}O_2$ in CD_3CN to afford a Fe(III)$_2$(μ-^{18}OD)$_2$ complex **2** which incorporates isotopic labels derived from dioxygen and acetonitrile solvent. It is suggested that an unobserved Fe-oxo intermediate capable of abstracting a H-atom from acetonitrile forms en route to **2**. Consistent with this, iodosylbenzene (PhIO) also reacts with **1** in CD_3CN to afford deuterated Fe(III)$_2$(μ-OD)$_2$ **2**. Dihydroxo-bridged **2** also abstracts H-atoms from substrates (DHA) containing weaker C−H bonds.

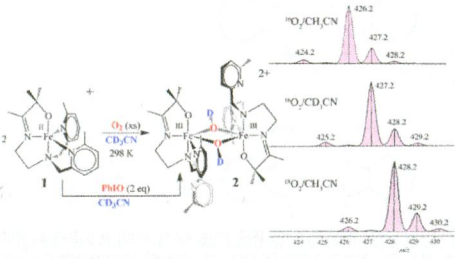

13332 S dx.doi.org/10.1021/ic401191e

Systematic Study of the Luminescent Europium-Based Nonanuclear Clusters with Modified 2-Hydroxybenzophenone Ligands

Bin Zhang, Ting Xiao, Chunmei Liu, Qian Li, Yanyan Zhu, Mingsheng Tang, Chenxia Du,* and Maoping Song*

Six novel diabolo-shaped nonanuclear Eu(III) clusters have been successfully obtained with 2-hydroxybenzophenone derivatives as ancillary ligands through a ligand-controlled hydrolytic approach. A correlation between luminescent efficiencies of Eu(III) complexes and the electronic features of the ligands has been proven.

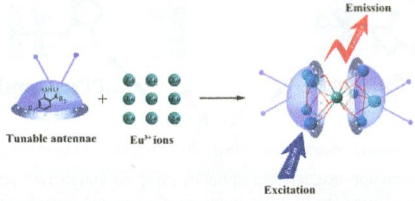

13341 S dx.doi.org/10.1021/ic4013075

Crystal Structures of Manganese and Cobalt Dichloride Monohydrate and Deuteration Effects on Magnetic Behavior

S. Pagola, K. T. Trowell, K. C. Havas, Z. D. Reed, D. G. Chan, M. J. Van Dongen, and G. C. DeFotis*

Crystal structures of $CoCl_2 \cdot H_2O$ and other unfamiliar monohydrate compounds, including deuterated forms, are determined. Common structures exhibit novel double chains from reorganization of coordination spheres and simpler chains in dihydrates. The magnetism of deuterated compounds is studied, revealing lowered magnetic dimensionality from weakened interchain exchange as in H_2O systems. Remarkably, while cobalt compounds show no detectable difference in behavior for H_2O vs D_2O, significant differences appear for manganese compounds, and an unexpected color change.

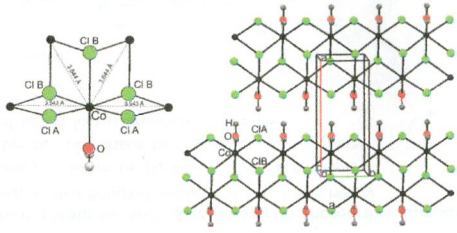

13351 dx.doi.org/10.1021/ic402417h

Exchange Coupling and Its Chemical Trend Studied by High-Frequency EPR on Heterometallic [Ln_2Ni] Complexes

Atsushi Okazawa, Takashi Shimada, Norimichi Kojima, Shunsuke Yoshii, Hiroyuki Nojiri, and Takayuki Ishida*

We applied high-frequency electron paramagnetic resonance to trinuclear 4f–3d heterometallic complexes, [{Ln-$(hfac)_3$}$_2${Ni$(dpk)_2(py)_2$}] (abbreviated as [Ln_2Ni]; Ln = Y, Gd, Tb, and Ho), and determined the exchange parameter J_{Ln-Ni} as well as nickel(II) zero-field splitting parameters. In contrast to the antiferromagnetic Dy analogue, ferromagnetic couplings were precisely characterized as J_{Gd-Ni}/k_B = +0.301(4) K, J_{Tb-Ni}/k_B = +0.216(12) K, and J_{Ho-Ni}/k_B = +0.110(3) K (defined as $-J_{Ln-Ni}\sum J_{Ln}{}^{z}S_{Ni}$).

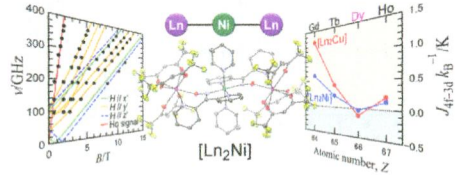

13356 dx.doi.org/10.1021/ic4014834

Synthetic Route to Metal Nitrides: High-Pressure Solid-State Metathesis Reaction

Li Lei,* Wenwen Yin, Xiaodong Jiang, Sen Lin,* and Duanwei He*

High-pressure solid-state metathesis (HPSSM) reactions occur between boron nitride (BN) and ternary metal oxides AMO (A = alkali or alkaline-earth metal and M = main group or transitional metal). The reaction results in a wide variety of important metal nitrides, including GaN, CrN, W_xN, Mo_xN, VN, Fe_3N, and Re_3N. In the reaction process, pressure opens different reaction pathways that have lower reaction enthalpy ΔH and higher activation energy E_a.

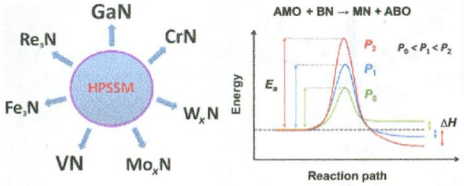

13363 dx.doi.org/10.1021/ic401487q

Magnetic Structure and Electromagnetic Properties of LnCrAsO with a ZrCuSiAs-type Structure (Ln = La, Ce, Pr, and Nd)

Sang-Won Park, Hiroshi Mizoguchi, Katsuaki Kodama, Shin-ichi Shamoto, Toshiya Otomo, Satoru Matsuishi, Toshio Kamiya, and Hideo Hosono*

We report the synthesis, structure, and electromagnetic properties of Cr-based layered oxyarsenides LnCrAsO (Ln = La, Ce, Pr, and Nd) with a ZrCuSiAs-type structure. All LnCrAsO samples showed metallic electronic conduction. Electron doping in LaCrAsO by Mn-substitution for the Cr sites gave rise to a metal–insulator transition. Analysis of powder neutron diffraction data revealed that LaCrAsO had G-type antiferromagnetic (AFM) ordering.

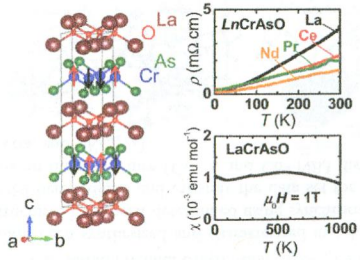

13369 S dx.doi.org/10.1021/ic402453p

The $(N_4C_2)^{2-}$ Donor Set as Promising Motif for Bis(tridentate) Iron(II) Photoactive Compounds

Isabelle M. Dixon,* Fabienne Alary, Martial Boggio-Pasqua, and Jean-Louis Heully

Iron(II) bis(1,3-di-2-pyridylbenzene) is shown by DFT and TDDFT to display promising photophysical properties by comparison to $Fe(tpy)_2^{2+}$. No tendency toward thermal or photochemical ligand loss is expected for the bis-(cyclometalated) compound.

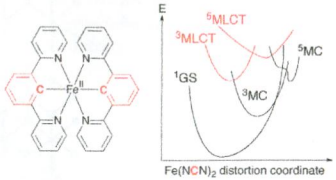

13375 S dx.doi.org/10.1021/ic401673z

Preferential Behavior on Donating Atoms of an Ambidentate Ligand 2-Methylisothiazol-3(2*H*)-one in Its Metal Complexes

Masaru Kato, Kei Unoura, Toshiyuki Takayanagi, Yasuhisa Ikeda, Takashi Fujihara, and Akira Nagasawa*

Five metal complexes of 2-methylisothiazol-3(2*H*)-one (MIO), $[Co^{III}(NH_3)_5(MIO)]^{3+}$, $[Ru^{II}(NH_3)_5(MIO)]^{2+}$, $[Ru^{III}(NH_3)_5(MIO)]^{3+}$, $[Pt^{II}Cl_3(MIO)]^-$, and *trans*-$[U^{VI}O_2(NO_3)_2(MIO)_2]$, have been synthesized, and their structures have been determined by single-crystal X-ray analysis. The X-ray crystal structures revealed that MIO showed preferential behavior on its donating sites in the metal complexes: MIO coordinates to the metal centers through its oxygen atom in the cobalt(III), ruthenium(III), and uranium(VI) complexes but through its sulfur atom in the ruthenium(II) and platinum(III) complexes. We also determined various physical parameters on MIO to study the electron-donating abilities of MIO.

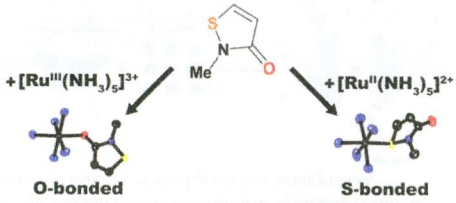

13384 S dx.doi.org/10.1021/ic401720e

Digermylene Oxide Complexes: Facile Synthesis and Reactivity

Rahul Kumar Siwatch, Dhirendra Yadav, Goutam Mukherjee, Gopalan Rajaraman, and Selvarajan Nagendran*

The conversion of aminotroponiminatogermylene monochlorides **1** and **2** to the corresponding digermylene oxides **3** and **4** has been achieved using a facile synthetic route. By carrying out the first direct reactivity on a digermylene oxide, we obtained novel germaacid anhydride complexes **5** and **6** with (S)Ge−O−Ge(S) and (Se)Ge−O−Ge(Se) moieties, respectively. Further, the bonding features in compounds **3** and **5**-**6** have been analyzed for the first time through DFT and AIM calculations.

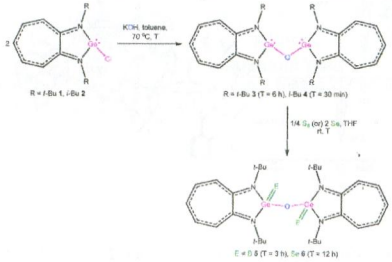

13392 S

dx.doi.org/10.1021/ic401715e

Trans and Cis Effects of Axial Fluoroalkyl Ligands in Vitamin B_{12} Analogues: Relationship between Alkyl- and Fluoroalkyl-Cobalamins

Lucio Randaccio, Giovanna Brancatelli, Nicola Demitri, Renata Dreos, Neal Hickey, Patrizia Siega, and Silvano Geremia*

CF_3CH_2Cbl, CF_2HCbl, and **CF_3Cbl** have been synthesized and characterized in solution by ^1H NMR and UV–vis spectroscopy, and their X-ray crystal structures have been determined using synchrotron radiation. This analysis substantially confirms and, with the new data reported here, adjusts and expands the data set for correlations between trans and cis influences of the β-ligand of cobalamins on their structure (Co–X and Co–NB3 distances and corrin fold angle) and properties (UV–vis spectra, NMR spectra, and $pK_{base\text{-}off}$).

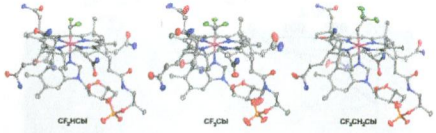

13402 S

dx.doi.org/10.1021/ic401710j

Investigation on NMR Relaxivity of Nano-Sized Cyano-Bridged Coordination Polymers

Marine Perrier, Samir Kenouche, Jêrôme Long, Kalaivani Thangavel, Joulia Larionova,* Christophe Goze-Bac, Alessandro Lascialfari, Manuel Mariani, Nathalie Baril, Christian Guérin, Bruno Donnadieu, Alexander Trifonov, and Yannick Guari

NMR relaxivity investigations have been performed on a family of nanosized cyano-bridged coordination polymers showing that $Gd^{3+}/[Fe(CN)_6]^{3-}$ nanoparticles present high MRI contrast efficiency and may be considered as potential contrast agents.

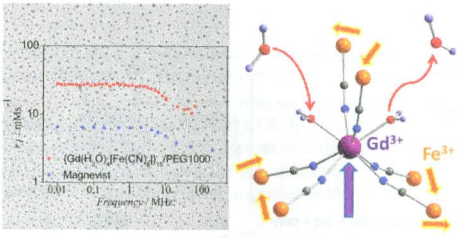

13415 S

dx.doi.org/10.1021/ic401752n

Role of Spin State and Ligand Charge in Coordination Patterns in Complexes of 2,6-Diacetylpyridinebis(semioxamazide) with 3d-Block Metal Ions: A Density Functional Theory Study

Stepan Stepanović, Ljubica Andjelković, Matija Zlatar, Katarina Andjelković, Maja Gruden-Pavlović,* and Marcel Swart*

Changes in the spin state lead to completely different five/seven-coordination modes for acylhydrazone complexes with some 3d metals, which can be understood based on a detailed computational study on the structures, spin states, and molecular orbitals of these complexes.

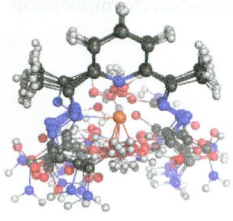

13424 Ⓢ dx.doi.org/10.1021/ic4017504

Vanadium Thiolate Complexes for Efficient and Selective Sulfoxidation Catalysis: A Mechanistic Investigation

Nikita Hall, Maylis Orio,* Adeline Jorge-Robin, Béatrice Gennaro, Caroline Marchi-Delapierre, and Carole Duboc*

Two alkyl thiolate vanadium complexes have shown their ability to catalyze the fast and selective oxidation of sulfide into sulfoxide. A ^{51}V NMR and EPR spectroscopic investigation combined with theoretical calculations has revealed that the structure of the *cis*-oxo peroxo V^V intermediate species can partly explain the difference in reactivity and stability between both catalysts.

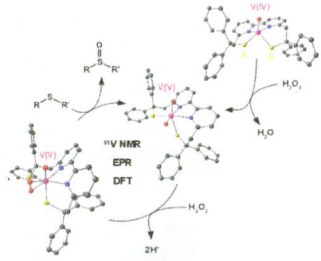

13432 Ⓢ dx.doi.org/10.1021/ic401810x

Selective Hg^{2+} Sensing Behaviors of Rhodamine Derivatives with Extended Conjugation Based on Two Successive Ring-Opening Processes

Chunyan Wang and Keith Man-Chung Wong*

A novel class of rhodamine derivatives with two spirolactam moieties have been synthesized, and their two stereoisomers of *cis*- and *trans*-forms have been successfully separated and isolated, as well as structurally characterized by X-ray crystallography. Different solution color, electronic absorption and emission responses attributed to the successive ring-openings of two spirolactam moieties were observed upon addition of various concentrations of mercury(II) ion.

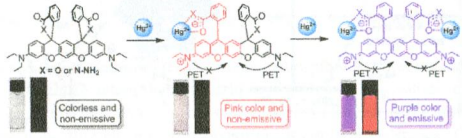

13442 Ⓢ dx.doi.org/10.1021/ic401819t

A Combined Experimental and Theoretical Investigation on the Role of Halide Ligands on the Catecholase-like Activity of Mononuclear Nickel(II) Complexes with a Phenol-Based Tridentate Ligand

Jaydeep Adhikary, Prateeti Chakraborty, Sudhanshu Das, Tanmay Chattopadhyay, Antonio Bauzá, Shyamal Kumar Chattopadhyay, Bipinbihari Ghosh, Franz A. Mautner,* Antonio Frontera,* and Debasis Das*

How a small change of the coordination environment may be instrumental in bringing about a spectacular difference in the catalytic activity of tridentate Schiff-base ligand complexes of nickel(II) halides has been explored by combined experimental and theoretical investigations.

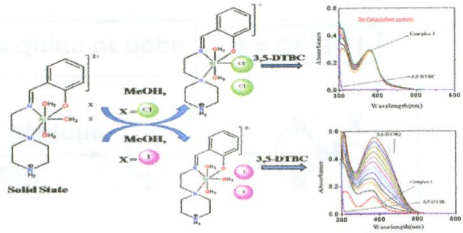

13453 S dx.doi.org/10.1021/ic401783c

Iridium(III) Hydrido N-Heterocyclic Carbene–Phosphine Complexes as Catalysts in Magnetization Transfer Reactions

Marianna Fekete, Oliver Bayfield, Simon B. Duckett,* Sam Hart, Ryan E. Mewis, Natalie Pridmore, Peter J. Rayner, and Adrian Whitwood

para-Hydrogen enables NMR characterization of the reaction intermediates via signal amplification by reversible exchange.

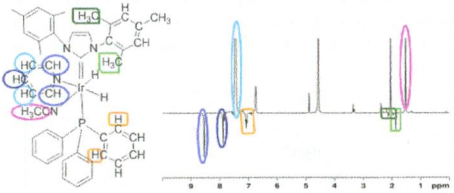

13462 S dx.doi.org/10.1021/ic4018344

Switchable Magnetism: Neutron Diffraction Studies of the Desolvated Coordination Polymer $Co_3(OH)_2(C_4O_4)_2$

Richard A. Mole,* Muhammad A. Nadeem, John A. Stride, Vanessa K. Peterson, and Paul T. Wood

The magnetic structure of the two ordered phases of $Co_3(OH)_2(C_4O_4)_2$ have been determined by neutron diffraction. This shows that the magnetic behavior changes significantly on dehydrating $Co_3(OH)_2(C_4O_4)_2{\cdot}3H_2O$; this is discussed in the context of the effect of the structure changes on the magnetic properties. In particular, the combination of changes in single-ion anisotropy and frustration are shown to drive the system to have a net magnetic moment.

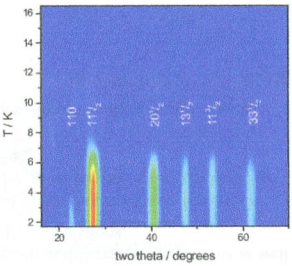

13469 S dx.doi.org/10.1021/ic401867c

Crystal Structures and Photoluminescence across the $La_2Si_2O_7$–$Ho_2Si_2O_7$ System

Alberto J. Fernández-Carrión, Mathieu Allix, Manuel Ocaña, Jorge García-Sevillano, Fernando Cusso, Andrew N. Fitch, Emmanuelle Suard, and Ana I. Becerro*

The $La_2Si_2O_7$–$Ho_2Si_2O_7$ system displays a solid solubility region of G-$(La,Ho)_2Si_2O_7$ which extends to the $La_{0.6}Ho_{1.4}Si_2O_7$ composition. Compositions richer in Ho^{3+} show a two-phase domain $(G+\delta)$, while δ-$(La,Ho)_2Si_2O_7$ is the stable phase for Ho^{3+} contents higher than $La_{0.2}Ho_{1.8}Si_2O_7$. A preferential occupation of Ho for the RE2 site of the G-unit cell is observed. Luminescence measurements have shown that the lifetimes remain unchanged in the range 0.5% < $[Ho^{3+}]$ < 10%, and only above this value does concentration quenching become operative.

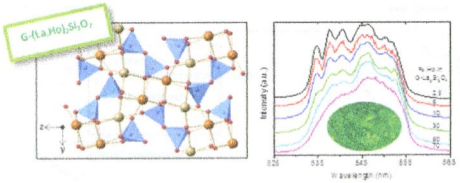

13480 dx.doi.org/10.1021/ic4018745

Bismuth–Halide Oxidative Addition and Bismuth–Carbon Reductive Elimination in Platinum Complexes Containing Chelating Diphosphine Ligands

S. Masoud Nabavizadeh,* Fatemeh Niroomand Hosseini,* Negar Nejabat, and Zahra Parsa

The reaction of organoplatinum(II) complexes $[PtMe_2(P{-}P)]$, P– P = dppm or dppe, with bismuth trihalides proceeds through bismuth–halide oxidative addition and bismuth–carbon reductive elimination reactions to yield a mixture of the platinum(II) complexes.

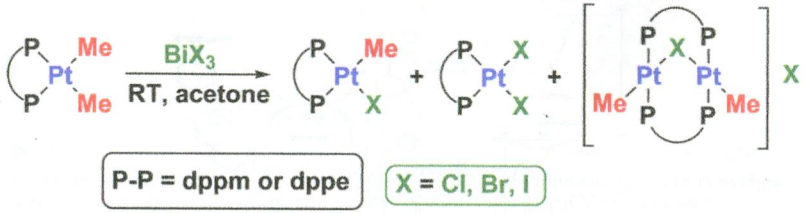

13490 S dx.doi.org/10.1021/ic4018823

An Inorganic Chromophore Based on a Molecular Oxide Supported Metal Carbonyl Cluster: $[P_2W_{17}O_{61}\{Re(CO)_3\}_3\{ORb(H_2O)\}(\mu_3\text{-}OH)]^{9-}$

Chongchao Zhao, William Rodríguez-Córdoba, Alexey L. Kaledin, Ye Yang, Yurii V. Geletii, Tianquan Lian,* Djamaladdin G. Musaev,* and Craig L. Hill*

A dyadic complex, $[P_2W_{17}O_{61}\{Re(CO)_3\}_3\{ORb(H_2O)\}(\mu_3\text{-}OH)]^{9-}$, comprising a trirhenium carbonyl cluster electron donor, and a polyoxometalate support electron acceptor has been synthesized and characterized. The intramolecular electron transfer, referred to as metal-to-polyoxometalate charge-transfer (MPCT), was thoroughly characterized by computational modeling and laser optical spectroscopy.

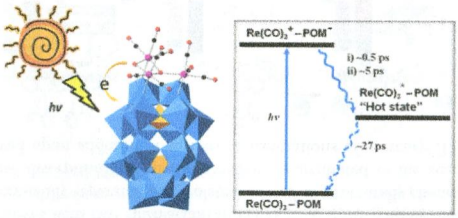

Intramolecular Metal-to-Polyoxometalate Charge-Transfer

13496 S dx.doi.org/10.1021/ic401907k

Mechanism-Based Inactivation of Cytochromes by Furan Epoxide: Unraveling the Molecular Mechanism

Nikhil Taxak, Sourav Kalra, and Prasad V. Bharatam*

The bioinorganic chemistry of furan epoxidation and competitive reactions of reactive furan epoxide metabolite are discussed. Mechanism-based inactivation (MBI) of cytochromes (CYPs) via covalent modification of amino acids by the furan epoxide metabolite is studied, and the factors favoring MBI are reported. Anionic active site nucleophilic residues cause epoxide ring opening, leading to irreversible MBI. The reaction pathway is supported by the heme center and occurs favorably in the absence of the competitive hydrolysis reaction.

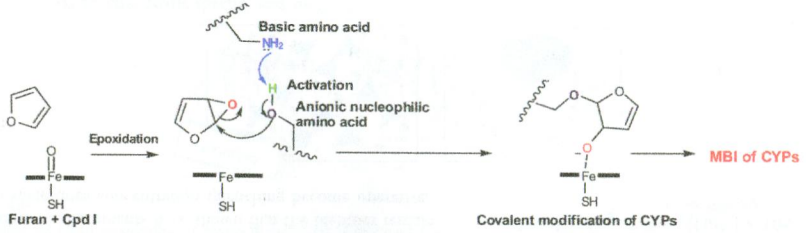

13509 S dx.doi.org/10.1021/ic4019162

Copper(I) Complexes Based on Five-Membered P^N Heterocycles: Structural Diversity Linked to Exciting Luminescence Properties

Daniel M. Zink, Thomas Baumann,* Jana Friedrichs, Martin Nieger, and Stefan Bräse*

Various highly luminescent copper(I) compounds showing different structural motifs have been synthesized by using bridging P^N ligands bearing five-membered heterocyclic moieties. Dinuclear and tetranuclear complex structures were confirmed by X-ray analysis. Electron-poor and electron-rich nitrogen-containing heterocycles have been used to shift the emission from deep blue (458 nm) to orange (617 nm). The photophysical characteristics were investigated in different environments as well as at different temperatures, and the photophysical interpretations are supported by DFT calculations.

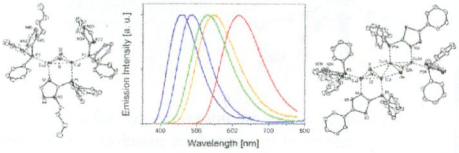

13521 S dx.doi.org/10.1021/ic401972g

Isostructural Nuclear and Luminescent Probes Derived From Stabilized [2 + 1] Rhenium(I)/Technetium(I) Organometallic Complexes

Tamil Selvi Pitchumony, Laura Banevicius, Nancy Janzen, Jon Zubieta, and John F. Valliant*

Methods for preparing ^{99m}Tc analogues of luminescent [2 + 1] Re(I) complexes were developed to establish a new class of isostructural nuclear and optical probes. The plasma stabilities of the ^{99m}Tc complexes were evaluated, where the basicity of the monodentate pyridine type ligand has a significant impact with half-lives ranging from 2 to 20 h. The radioactive complexes can be used to quantitate cell uptake, which was demonstrated using ^{99m}Tc analogues of Re(I)-based mitochondrial targeting dyes.

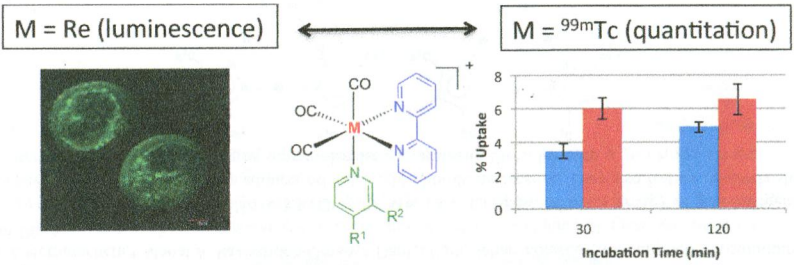

13529 S dx.doi.org/10.1021/ic401973k

Anticancer C,N-Cycloplatinated(II) Complexes Containing Fluorinated Phosphine Ligands: Synthesis, Structural Characterization, and Biological Activity

Natalia Cutillas, Alexandra Martínez, Gorakh S. Yellol, Venancio Rodríguez, Ana Zamora, Mónica Pedreño, Antonio Donaire, Christoph Janiak, and José Ruiz*

New potent cytotoxic C,N-cyclometalated platinum(II) fluorinated phosphine complexes have been prepared. In some cases at 48 h incubation, they were 17-fold more active than cisplatin in T47D, and IC_{50} values in A2780 are in the same order of magnitude than cisplatin. On the other hand, very low resistance factors (RF) in A2780cisR (cisplatin-resistant ovarian carcinoma) at 48 h were observed indicating efficient circumvention of cisplatin resistance. They arrest cell growth in G0/G1 phase in contrast to cisplatin (S phase) with a high incidence of late-stage apoptosis.

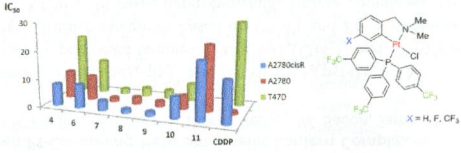

13536 dx.doi.org/10.1021/ic401997w

Modeling the Magnetic Properties and Mössbauer Spectra of Multifunctional Magnetic Materials Obtained by Insertion of a Spin-Crossover Fe(III) Complex into Bimetallic Oxalate-Based Ferromagnets

S. M. Ostrovsky, O. S. Reu, A. V. Palii, M. Clemente-León, E. Coronado, J. C. Waerenborgh, and S. I. Klokishner*

A theoretical microscopic approach to describe the magnetic and spectroscopic behavior of multifunctional hybrid materials that demonstrate spin crossover and ferromagnetic ordering is presented. For all complexes under study, a qualitative and quantitative interpretation was given of the experimental data on the temperature dependence of the magnetic susceptibility and Mössbauer spectra. The calculations performed apparently show a recognizable trend in the magnetic and spectroscopic behaviors induced by different solvent molecules.

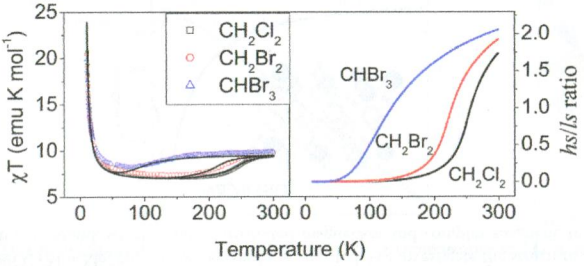

13546 dx.doi.org/10.1021/ic402501k

C–H Oxidation by H_2O_2 and O_2 Catalyzed by a Non-Heme Iron Complex with a Sterically Encumbered Tetradentate N-Donor Ligand

Qiao Zhang, John D. Gorden, and Christian R. Goldsmith*

A complex with a sterically encumbered tetradentate N-donor ligand catalyzes the oxidation of hydrocarbons by hydrogen peroxide and dioxygen. The ligand appears to destabilize the oxidant generated from hydrogen peroxide; the remaining oxidation is directed towards the secondary carbons of most of the investigated substrates. The catalyzed oxidation of hydrocarbons by dioxygen results in few dehydrogenated products relative to previously characterized systems.

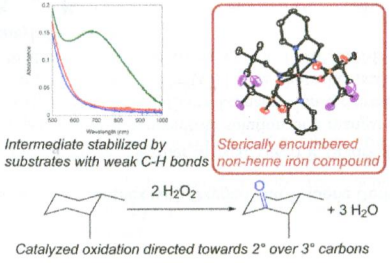

13555 S dx.doi.org/10.1021/ic4020459

Controlling the Dipole–Dipole Interactions between Terbium(III) Phthalocyaninato Triple-Decker Moieties through Spatial Control Using a Fused Phthalocyaninato Ligand

Takaumi Morita, Keiichi Katoh,* Brian K. Breedlove, and Masahiro Yamashita*

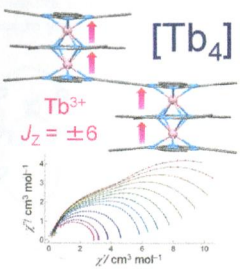

Using a fused phthalocyanine ligand to control the spatial arrangement of Tb^{III} moieties in Tb^{III} single-molecule magnets (SMMs), we could control the dipole–dipole interactions in the molecules and prepared the first tetranuclear Tb^{III} SMM complex, [**Tb_4**]. [**Tb_4**] can be described as a weakly ferromagnetically coupled dimer of triple-decker $Tb_2(obPc)_3$ complexes with strong dipole–dipole interactions in the triple-decker moieties and weak ones through the fused phthalocyaninato ligand linking the two triple-decker complexes. Through a better understanding of the magnetic dipole–dipole interactions obtained in these studies, we have developed a new strategy for preparing Tb^{III} SMMs.

13562 S dx.doi.org/10.1021/ic402075y

Pt···Pt vs Pt···S Contacts Between Pt-Containing Heterobimetallic Lantern Complexes

Frederick G. Baddour, Stephanie R. Fiedler, Matthew P. Shores, Jeffrey W. Bacon, James A. Golen, Arnold L. Rheingold, and Linda H. Doerrer*

The new heterobimetallic complexes $[PtM(SAc)_4(py)]$ and $[PtM(SAc)_4(pyNH_2)]$ (M = Co, Ni, Zn) are analyzed in comparison with two other previously published families, $[PtM(tba)_4(OH_2)]$ and $[PtM(SAc)_4(L)]$, L = OH_2, $pyNO_2$. Structures are divided among three distinct categories based on Pt···Pt and Pt···S distances and the presence of antiferromagnetic coupling or not. A trio of Pt-based heterobimetallic lantern complexes $[(py)PtM(SAc)_4(py)]$ (M = Co, Ni, Zn) with unusual octahedral coordination of Pt(II) was also prepared

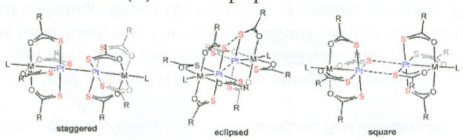

13576 S dx.doi.org/10.1021/ic402080y

Trinuclear Copper(I) and Silver(I) Adducts of 4-Chloro-3,5-bis(trifluoromethyl)pyrazolate and 4-Bromo-3,5-bis(trifluoromethyl)pyrazolate

Champika V. Hettiarachchi,* Manal A. Rawashdeh-Omary,* Daniel Korir, Jehan Kohistani, Muhammed Yousufuddin, and H. V. Rasika Dias*

Trinuclear copper and silver complexes $\{[4\text{-X-3,5-}(CF_3)_2Pz]M\}_3$ (X = Cl or Br, M = Cu or Ag) of poly halogenated pyrazolates have been synthesized. These adducts exhibit bright photoluminescence. They also feature relatively short M···Cl or M···Br intertrimer separations leading to supramolecular aggregates in the solid state.

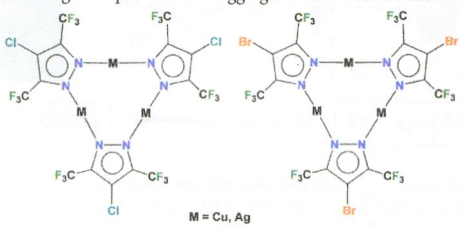

13584 S dx.doi.org/10.1021/ic402105m

Dispersion Force Stabilized Two-Coordinate Transition Metal–Amido Complexes of the –N(SiMe$_3$)Dipp (Dipp = C$_6$H$_3$-2,6-Pr$^i_2$) Ligand: Structural, Spectroscopic, Magnetic, and Computational Studies

Chun-Yi Lin, Jing-Dong Guo, James C. Fettinger, Shigeru Nagase,* Fernande Grandjean, Gary J. Long,* Nicholas F. Chilton, and Philip P. Power*

Structural, spectroscopic, and computational studies of M{N(SiMe$_3$)Dipp}$_2$ (M = Fe, Co, or Ni; Dipp = C$_6$H$_3$-2,6-Pr$^i_2$) show that their planar M{N(Si)(Cipso)}$_2$ core structures are stabilized by dispersion forces between the C–H moieties of the ligand substituents. The attempted synthesis of their chromium analogue yielded the unusual tetrametallic species [Cr{N(SiMe$_2$CH$_2$)Dipp}$_2$Cr]$_2$(THF), which was formed by dehydrogenation of a Si–Me moiety from each amido ligand.

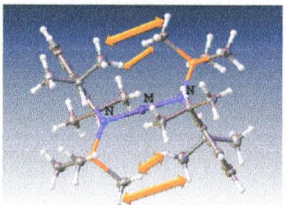

13594 S dx.doi.org/10.1021/ic402121j

Photochemical Oxidation of a Manganese(III) Complex with Oxygen and Toluene Derivatives to Form a Manganese(V)-Oxo Complex

Jieun Jung, Kei Ohkubo, Katharine A. Prokop-Prigge, Heather M. Neu, David P. Goldberg,* and Shunichi Fukuzumi*

Visible light photoirradiation of an oxygen-saturated benzonitrile solution of a manganese(III) corrolazine complex [(TBP$_8$Cz)Mn^{III} (**1**): [TBP$_8$Cz = octakis(*p*-*tert*-butylphenyl)corrolazinato^{3-}] in the presence of toluene derivatives resulted in formation of the manganese(V)-oxo complex [(TBP$_8$Cz)Mn^V(O)]. The photochemical oxidation of (TBP$_8$Cz)Mn^{III} with O$_2$ and hexamethylbenzene (HMB) led to the isosbestic conversion of **1** to (TBP$_8$Cz)Mn^V(O), accompanied by the selective oxidation of HMB to pentamethylbenzyl alcohol (87%).

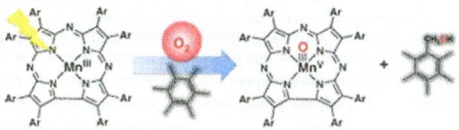

13605 S dx.doi.org/10.1021/ic402131e

Structure and Magnetic Properties of the α-NaFeO$_2$-Type Honeycomb Compound Na$_3$Ni$_2$BiO$_6$

Elizabeth M. Seibel,* J. H. Roudebush, Hui Wu, Qingzhen Huang, Mazhar N. Ali, Huiwen Ji, and R. J. Cava

The synthesis of Na$_3M_2$BiO$_6$ (*M* = Mg, Ni, Zn) honeycombs is reported. We investigate the structure and magnetic properties of the nickel honeycomb compound, which displays frustrated magnetism and complex magnetic transitions.

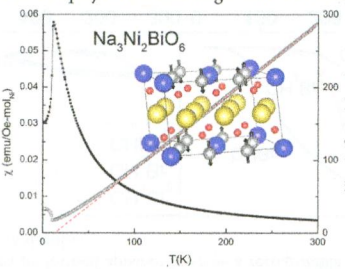

13612 S dx.doi.org/10.1021/ic402133c

Square-Planar Cu(II) Diketiminate Complexes in Lactide Polymerization

Todd J. J. Whitehorne and Frank Schaper*

Copper(II) bisdiketiminate complexes catalyze the polymerization of lactide with very good activities in the presence of alcohol or with extremely high activities as the isolated heteroleptic alkoxide complex.

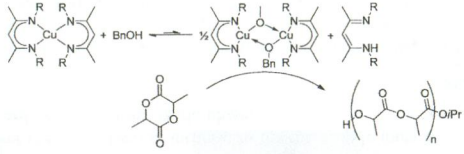

13623 S dx.doi.org/10.1021/ic402145k

Gold Network Structures in Rhombohedral and Monoclinic $Sr_2Au_6(Au,T)_3$ (T = Zn, Ga). A Transition via Relaxation

Trinath Mishra, Qisheng Lin, and John D. Corbett*

Decreases of effective valence electron counts via more Au/T mixing in the triangular units $(Au,T)_3$ in $SrAu_6(Au,T)_3$ (T = Zn, Ga) lead to symmetry breaking from trigonal $R\bar{3}c$ to monoclinic $C2/c$, as exemplified by these Zn structures.

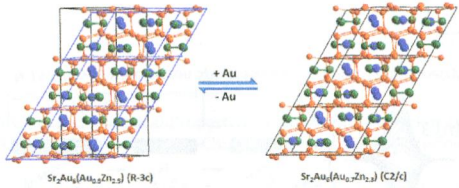

13631 S dx.doi.org/10.1021/ic402185s

$Yb_5Ga_2Sb_6$: A Mixed Valent and Narrow-Band Gap Material in the $RE_5M_2X_6$ Family

Udumula Subbarao, Sumanta Sarkar, Vijay Kumar Gudelli, V. Kanchana, G. Vaitheeswaran, and Sebastian C. Peter*

A new Zintl compound $Yb_5Ga_2Sb_6$ having mixed valent Yb was synthesized by the metal flux technique as well as high frequency induction heating. The crystal structure of $Yb_5Ga_2Sb_6$ was studied using single crystal X-ray diffraction data. Electrical resistivity and absorption studies suggest that $Yb_5Ga_2Sb_6$ is a narrow band gap semiconductor. Electron full-potential linear augmented plane wave calculations confirm the pseudo gap in the density of states revealing semimetallic character.

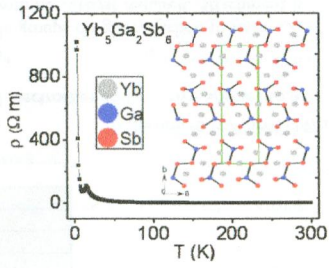

13639 S

dx.doi.org/10.1021/ic402208s

High-Temperature, High-Pressure Hydrothermal Synthesis, Crystal Structures, and Spectroscopic Studies of a Uranium(IV) Phosphate ($Na_{10}U_2P_6O_{24}$) and the Isotypic Cerium(IV) Phosphate ($Na_{10}Ce_2P_6O_{24}$)

Yu-Hsien Lai, Yu-Chih Chang, Tsz-Fung Wong, Wan-Ju Tai, Wen-Jung Chang, and Kwang-Hwa Lii*

A U(IV) phosphate and the isotypic Ce(IV) phosphate were synthesized under hydrothermal conditions at 570 °C and 160 MPa and characterized by single-crystal X-ray diffraction. Their three-dimensional structure is formed of MO_8 snub-disphenoidal polyhedra and PO_4 tetrahedra and contains intersecting 12-sided channels. The valence state of U was confirmed by UV−vis and U 4f X-ray photoelectron spectroscopy. The Ce compound is the first structurally characterized Ce(IV) phosphate with a P/Ce ratio of 3.

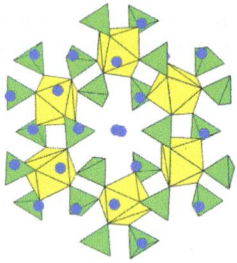

13644 S

dx.doi.org/10.1021/ic402214p

$SrGe_2B_2O_8$ and $Sr_3Ge_2B_6O_{16}$: Novel Strontium Borogermanates with Three-Dimensional and Layered Anionic Architectures

Yu-Cheng Hao, Chun-Li Hu, Xiang Xu, Fang Kong, and Jiang-Gao Mao*

Two new strontium borogermanates, $SrGe_2B_2O_8$ and $Sr_3Ge_2B_6O_{16}$, have been successfully synthesized through high-temperature solid state reactions. $SrGe_2B_2O_8$ features a novel three-dimensional $[Ge_2B_2O_8]^{2-}$ framework composed of alternative linkages of the B_2O_7 and Ge_2O_7 dimeric units with one-dimensional (1D) tunnels of eight-membered rings (MRs) along the *b* axis that are filled by the Sr^{2+} cations. $Sr_3Ge_2B_6O_{16}$ displays a layered structure composed of circular B_6O_{16} clusters interconnected by GeO_4 tetrahedra via corner sharing, forming 1D four- and six-MR tunnels along the *a* axis.

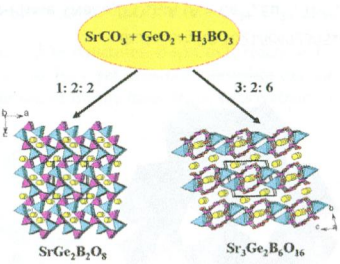

13651 S

dx.doi.org/10.1021/ic4022195

Synthesis of (TDAE)(O_2SSO_2)(s) and Discovery of (TDAE)(O_2SSSSO_2)(s) Containing the First Polythionite, $[O_2SSSSO_2]^{2-}$

Pablo Bruna, Andreas Decken, Scott Greer, Friedrich Grein, H. Donald B. Jenkins, Birgit Mueller, Jack Passmore,* Tressia A. P. Paulose, J. Mikko Rautiainen, Stephanie Richardson, and Melbourne J. Schriver

Preparation of analytically pure (TDAE)(O_2SSO_2)(s) by reaction of TDAE(l) and SO_2(g) also gives the corresponding salt of the new sulfur oxyanion $[O_2SSSSO_2]^{2-}$ as a byproduct.

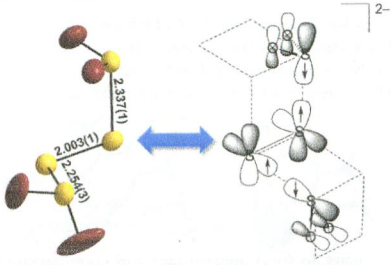

13663 dx.doi.org/10.1021/ic4022307

Biological Studies of Chalcogenolato-Bridged Dinuclear Half-Sandwich Complexes

Justin P. Johnpeter, Gajendra Gupta, Jerald Mahesh Kumar, Gunda Srinivas, Narayana Nagesh,* and Bruno Therrien*

A series of thiolato-, selenolato-, and tellurolato-bridged dinuclear half-sandwich complexes have been synthesized and their biological activities studied by cell biology and biophysical experiments. The nature of the chalcogenolato-bridge (S > Se > Te) appears to be more important than the nature of the metal centers (Ru > Rh > Ir) on the biological activity: The most active derivative is the cationic trithiolato-bridged diruthenium complex $[(\eta^6\text{-}p\text{-}MeC_6H_4Pr^i)_2Ru_2(\mu\text{-}SC_6H_5)_3]^+$, with half maximal inhibitory concentrations in the nanomolar range.

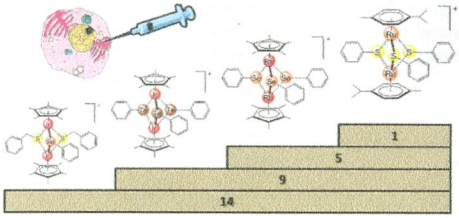

13674 (S) dx.doi.org/10.1021/ic402247n

The Electrode as Organolithium Reagent: Catalyst-Free Covalent Attachment of Electrochemically Active Species to an Azide-Terminated Glassy Carbon Electrode Surface

Atanu K. Das, Mark H. Engelhard, Fei Liu, R. Morris Bullock, and John A. S. Roberts*

Lithium acetylide–ethylenediamine undergoes catalyst-free cycloaddition wth azide groups on glassy carbon to form 1,2,3-triazolyllithium surface groups that are active for C–C coupling reactions, again with no catalyst required. Attachment is demonstrated with (6-iodohexyl)ferrocene and ferrocenecarboxaldehyde. Voltammetry, X-ray photoelectron spectra, and reflectance infrared spectra are presented. Results are compared side by side with the more common Cu(I)-catalyzed alkyne–azide coupling (CuAAC) route.

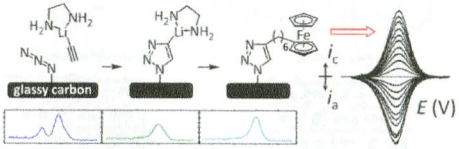

13685 (S) dx.doi.org/10.1021/ic402248y

Design of One-Dimensional Coordination Networks from a Macrocyclic {3d-4f} Single-Molecule Magnet Precursor Linked by $[W(CN)_8]^{3-}$ Anions

Sébastien Dhers, Humphrey L. C. Feltham, Rodolphe Clérac,* and Sally Brooker*

Two different 1D-chain arrangements, stepped (left, **2**) and square-wave (right, **3**) are reproducibly obtained from assembling the macrocyclic SMM $[Cu_3Tb(L^{Pr})]^{3+}$ with $[W(CN)_8]^{3-}$. Both compounds display an antiferromagnetic ground state, but feature metamagnetic and antiferromagnetic (T, H) phase diagrams for **2** and **3** respectively. Remarkably the slow dynamics of the magnetization intrinsic to the macrocycle units is preserved in **2** even in the 3D ordered antiferromagnetic phase.

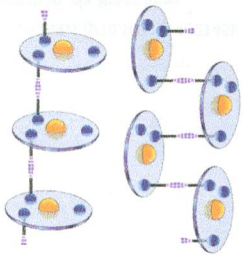

13692 S dx.doi.org/10.1021/ic402255m

Understanding the Mechanism of Polymerization of ε-Caprolactone Catalyzed by Aluminum Salen Complexes

Maria O. Miranda, Yvonne DePorre, Hugo Vazquez-Lima, Michelle A. Johnson, Daniel J. Marell, Christopher J. Cramer,* and William B. Tolman*

Experimental kinetics studies combined with DFT calculations revealed microscopic details of the reaction pathway for polymerization of ε-caprolactone (CL) by salen-aluminum catalysts.

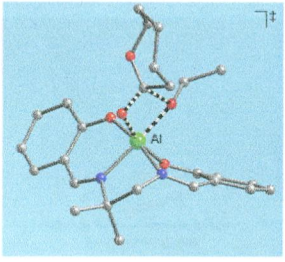

13702 S dx.doi.org/10.1021/ic402296t

Wells–Dawson Cages as Molecular Refrigerants

Eufemio Moreno Pineda, Floriana Tuna, Yan-Zhen Zheng, Richard E. P. Winpenny,* and Eric J. L. McInnes*

A series of $\{Ni_6Ln_6\}$ cages has been prepared using five different phosphonate ligands. The core, if the P sites are included, resembles the Wells–Dawson ion. Magnetic measurements show significant magnetic caloric effects for all compounds where Ln = Gd.

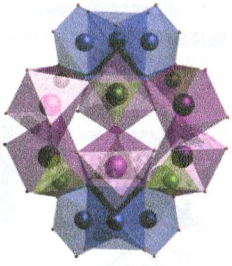

13708 S dx.doi.org/10.1021/ic402305x

Color-Tunable and White Luminescence Properties via Energy Transfer in Single-Phase $KNaCa_2(PO_4)_2$:A (A = Ce^{3+}, Eu^{2+}, Tb^{3+}, Mn^{2+}, Sm^{3+}) Phosphors

Dongling Geng, Mengmeng Shang, Yang Zhang, Hongzhou Lian, and Jun Lin*

A series of single-phase phosphors based on $KNaCa_2(PO_4)_2$ (KNCP):A (A = Ce^{3+}, Eu^{2+}, Tb^{3+}, Mn^{2+}, Sm^{3+}) have been prepared via a Pechini-type sol–gel method. Photoluminescence and cathodoluminescence properties of Ce^{3+}-, Eu^{2+}-, Tb^{3+}-, Mn^{2+}-, and Sm^{3+}-activated KNCP phosphors were investigated.

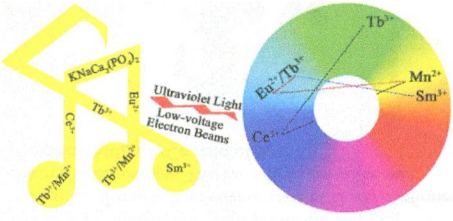

13719 S dx.doi.org/10.1021/ic402317g

Cobalt(III) Diazabutadiene Precursors for Metal Deposition: Nanoparticle and Thin Film Growth

Thomas Pugh, Samuel D. Cosham, Jeff A. Hamilton, Andrew J. Kingsley, and Andrew L. Johnson*

We report the synthesis and characterization of a family of cobalt(III) metal precursors, based around cyclopentadienyl and diazabutadiene ligands. Atmospheric pressure chemical vapor deposition (AP-CVD) was employed using the precursor cyclopentadienyl Cobalt(III) (di-isopropyl-diazabutadiene) **2a**, to synthesize thin films of metallic cobalt on silicon substrates under an atmosphere of hydrogen (H_2). Analysis of the thin films deposited at substrate temperatures of 250 °C, 275 °C, 325 °C, and 350 °C respectively by SEM and AFM reveal temperature dependent growth features.

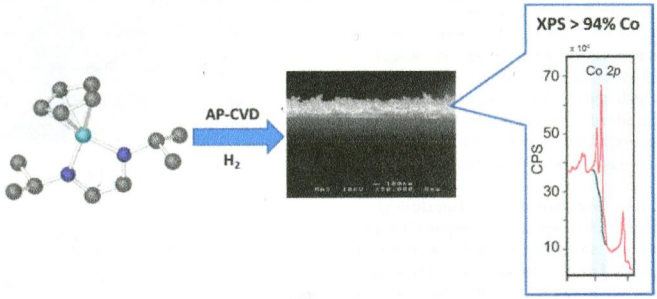

13730 S dx.doi.org/10.1021/ic402318k

Average and Local Structural Origins of the Optical Properties of the Nitride Phosphor $La_{3-x}Ce_xSi_6N_{11}$ ($0 < x \leq 3$)

Nathan C. George, Alexander Birkel, Jakoah Brgoch, Byung-Chul Hong, Alexander A. Mikhailovsky, Katharine Page, Anna Llobet, and Ram Seshadri*

The local structure of the nitride phosphor $La_{3-x}Ce_xSi_6N_{11}$ has been studied via several techniques, including solid-state ^{29}Si NMR, shown here. The two small peaks from the resonance of ^{29}Si nuclei near paramagnetic Ce^{3+} in the lattice allow the occupancy of Ce on the La site to be distinguished.

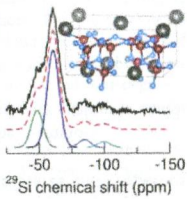

13742 S dx.doi.org/10.1021/ic402336n

Slow Spin Dynamics between Ferromagnetic Chains in a Pure-Inorganic Framework

Rénald David, Houria Kabbour, Silviu Colis, and Olivier Mentré*

$BaCo^{II}_2(As^{III}_3O_6)_2{\cdot}2(H_2O)$ is a unique case of pure-inorganic compounds with isolated ferromagnetic Ising canted chains. They diplay a metamagnetic reorientation at low field and slow spin dynamics.

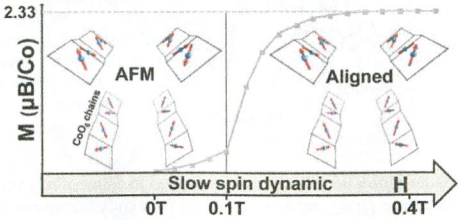

13751 S dx.doi.org/10.1021/ic402344m

Control of Bond-Strain-Induced Electronic Phase Transitions in Iron Perovskites

Ikuya Yamada,* Hidenobu Etani, Kazuki Tsuchida, Shohei Marukawa, Naoaki Hayashi, Takateru Kawakami, Masaichiro Mizumaki, Kenya Ohgushi, Yoshihiro Kusano, Jungeun Kim, Naruki Tsuji, Ryoji Takahashi, Norimasa Nishiyama, Toru Inoue, Tetsuo Irifune, and Mikio Takano

Unusual electronic phase transitions in the *A*-site ordered perovskites $Ln^{3+}Cu^{2+}{}_3Fe^{3.75+}{}_4O_{12}$ (*Ln*: lanthanide) are investigated. $LnCu_3Fe_4O_{12}$ with larger *Ln* ions (*Ln* = La, Pr, Nd, Sm, Eu, Gd, Tb) show an intersite charge transfer transition ($3Cu^{2+} + 4Fe^{3.75+} \rightarrow 3Cu^{3+} + 4Fe^{3+}$). In contrast, $LnCu_3Fe_4O_{12}$ with smaller *Ln* ions (*Ln* = Dy, Ho, Er, Tm Yb, Lu) transform into a charge-disproportionated ($8Fe^{3.75+} \rightarrow 5Fe^{3+} + 3Fe^{5+}$) and charge-ordered phase.

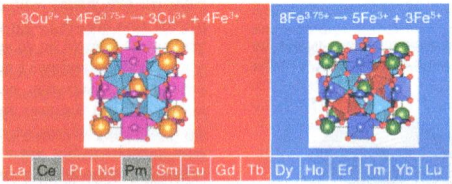

13762 S dx.doi.org/10.1021/ic402349r

Synthesis and Selective Topochemical Fluorination of the Cation and Anion-Vacancy Ordered phases Ba_2YCoO_5 and $Ba_3YCo_2O_{7.5}$

Kun Luo, T. Thao Tran, P. Shiv Halasyamani, and Michael A. Hayward*

Ba_2YCoO_5 and $Ba_3YCo_2O_{7.5}$ adopt cation-ordered and anion-vacancy ordered perovskite structures. Ba_2YCoO_5 reacts with CuF_2 under flowing oxygen by topochemically intercalating fluorine to form $Ba_2YCoO_5F_{0.42}$, yet does not intercalate oxygen even under pressure. The selective intercalation of fluorine but not oxygen is rationalized on the basis of the lattice strain of the oxidized product phases.

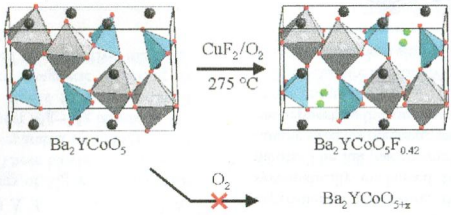

13770 S dx.doi.org/10.1021/ic402367c

Shedding Light on the Single-Molecule Magnet Behavior of Mononuclear Dy^{III} Complexes

Daniel Aravena and Eliseo Ruiz*

A set of mononuclear Dy^{III} complexes showing zero-field SMM, field-induced SMM, and no SMM behavior was studied by CASSCF-RASSI calculations. The role of ligand environment in SMM properties was rationalized in terms of electrostatic potentials caused by such ligands and with the arrangement of 4f electrons in the Dy^{III} center to reduce the electron repulsion with the ligand electrons. Low-symmetry environments are suggested for achieving SMM behavior.

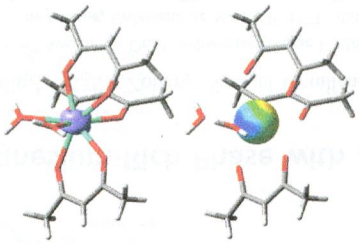

13779 Ⓢ dx.doi.org/10.1021/ic402485d

Thermal and Photoreductive Elimination from the Tellurium Center of π-Conjugated Tellurophenes

Elisa I. Carrera, Theresa M. McCormick, Marius J. Kapp, Alan J. Lough, and Dwight S. Seferos*

A conjugated tellurophene substituted with strong light-absorbing isoindigo units can undergo oxidative addition of halogens to form dibromo- and dichloro- Te(IV) compounds. These compounds can undergo thermal reductive elimination as well as photoreductive elimination using low-energy (505 nm) light to restore the Te(II) compound. Photochemical quantum yields near 0.20% are achieved. This is the first example of photoreductive elimination from a mononuclear tellurium compound and, in particular, a tellurophene.

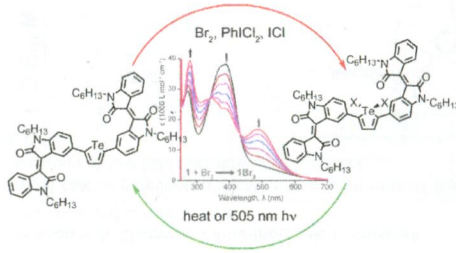

13791 Ⓢ dx.doi.org/10.1021/ic402038x

Transition Metal Complexes of 3-Amino-1-nitroguanidine as Laser Ignitible Primary Explosives: Structures and Properties

Niko Fischer, Manuel Joas, Thomas M. Klapötke,* and Jörg Stierstorfer

Plenty of new energetic transition metal (Co, Ni, Cu, ZN, Ag) complexes were synthesized using the 3-amino-1-nitroguanidine ligand in combination with oxygen-rich counterions. Some of the obtained (mostly) primary explosives could be successfully initiated by near-IR laser radiation.

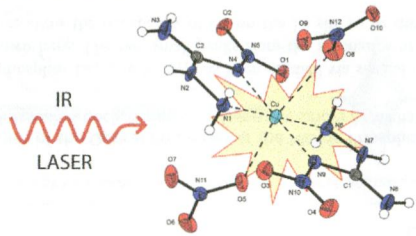

Ⓢ Supporting Information available via online article